Acta Materialia 241 (2022) 118375

Contents lists available at ScienceDirect

Acta Materialia

journal homepage: www.elsevier.com/locate/actamat

Full length article

Microscopic origin of the acceptor removal in neutron-irradiated Si detectors - An atomistic simulation study

P. López [a,*], M. Aboy [a], I. Santos [a], L.A. Marqués [a], M. Ullán [b], L. Pelaz [a]

[a] Departamento de Electricidad y Electrónica, Universidad de Valladolid, ETSI Telecomunicación, Paseo de Belén 15, Valladolid 47011, Spain
[b] Centro Nacional de Microelectrónica (IMB-CNM, CSIC), Campus UAB, Bellaterra 08193 (Barcelona), Spain

ARTICLE INFO

Article history:
Received 30 March 2022
Revised 14 September 2022
Accepted 21 September 2022
Available online 21 September 2022

Keywords:
Silicon
Atomistic simulations
Irradiation effect
Lattice defects
Acceptor removal

ABSTRACT

The improved radiation hardness of *p*-type Si detectors is hindered by the radiation-induced acceptor removal process, which is not fully understood yet. Through atomistic modeling of displacement damage and dopant interactions, we analyze the acceptor removal under neutron irradiation, providing physical insight into its microscopic origin. Our results show that the fast decay of the effective dopant concentration (N_{eff}) at low irradiation fluences is due to B deactivation caused by Si self-interstitials. The intriguing increase of the acceptor removal parameter with the initial dopant concentration ($N_{eff,0}$) is explained by the limited number of mobile Si self-interstitials that survive annihilation and clustering processes. The sublinear dependence of the removal parameter on $N_{eff,0}$ is associated to the inhomogeneity of damage for low $N_{eff,0}$ and the formation of B-interstitial clusters with several B atoms for high $N_{eff,0}$. The presence of O and C modifies B deactivation mechanisms due to the key role of B_iO defects and the trapping of vacancies and Si self-interstitials, but for the impurity concentrations analyzed in this work ([O] >> [C]) it has little effect on the overall amount of removed acceptors. At high irradiation fluences, the reported increase of N_{eff} is attributed to the formation of defect-related deep acceptors. From the analysis of the defect concentrations resulting from neutron irradiation and the occupancy of small clusters with acceptor levels reported in literature, we point out the tetra-vacancy cluster as one of the main contributors to N_{eff} with negative space charge.

1. Introduction

Si sensors fabricated on lowly doped *p*-type substrates are a technological solution adopted for the next generation of particle detectors. *P*-type sensors show an improved radiation hardness that makes them suitable to withstand the harsh radiation fields expected in high energy physics experiments [1]. One of the main effects of irradiation in Si devices is the so-called displacement damage. It arises from the generation of Si self-interstitials (I's) and vacancies (V's) when Si atoms are moved from their lattice positions. Radiation-induced defects have a strong impact on the detector electrical behavior due to an effective dopant concentration (N_{eff}) whose value may notably differ from that before irradiation [2]. As a consequence, the resistivity of the detector depleted region changes and the net space charge is modified, affecting the electric field profile and the full depletion voltage (V_{FD}). Radiation-induced changes on N_{eff} represent a serious challenge for the fabrication of radiation-hard *p*-type Si detectors, especially for novel architectures built on low resistivity Si, such as Low Gain Avalanche Detectors (LGAD) [3–5] and High-Voltage CMOS detectors (HV-CMOS) [6–9].

Recent works have addressed the experimental characterization of N_{eff} upon hadron irradiation in *p*-type sensors by measuring the variations on resistivity and V_{FD} with fluence [3,5,7–9]. As many detectors are expected to operate in cooled conditions for a lifetime of several years, accelerated annealing tests are used to analyze system dynamics. It is commonly assumed that a stable space charge, i.e. a constant value of N_{eff} over time, can be obtained after annealing for 80 min at 60 °C [10]. In these conditions, N_{eff} is strongly dependent on irradiation fluence. At low fluences, N_{eff} follows an exponential decay with fluence attributed to an acceptor removal process [2,10], i.e. the deactivation of dopants (usually B atoms) by displacement damage. The fast decay of N_{eff} is characterized by the so-called "acceptor removal constant" that reduces as the initial dopant concentration ($N_{eff,0}$) increases [4]. The mechanisms behind this dependence are still unknown, and it remains as one of the most intriguing features of acceptor removal. At high fluences, N_{eff} increases linearly with irradiation fluence, which is

* Corresponding author.
E-mail address: pedrol@ele.uva.es (P. López).

https://doi.org/10.1016/j.actamat.2022.118375

associated to the formation of defect-related deep acceptor levels [10,11]. Electrically active defects can be experimentally characterized to some extent by Deep Level Transient Spectroscopy (DLTS) and Thermally Stimulated Current (TSC) techniques [12]. However, the large variety of defect sizes and topologies hinders the identification of the defects responsible for the spectra peaks, and their usually small size prevents the direct observation by microscopy.

The modeling of radiation-induced changes on N_{eff} is complicated because of the large amount of defect-related energy levels observed after irradiation, and the difficulty in linking macroscopic effects with microscopic defects [12,13]. Most models attempt to simulate the electrical behavior of irradiated devices by posing a phenomenological description of the process. The acceptor removal is usually modeled with a few first order equations for defect reactions with dopants and impurities, and the use of several parameters to account for the generation of displacement damage and the formation of B defects [3,14,15]. The increase of N_{eff} at moderate fluences is simplified by assuming that the effects of displacement damage can be effectively represented by a few donor/acceptor energy levels in the Si bandgap, with parameters fitted to reproduce the macroscopic degradation of the detector electrical properties [16,17]. Although available empirical models could be fitted to reproduce the macroscopic behavior of devices to some extent, they do not provide insight on the physical mechanisms underlying the changes of N_{eff} with fluence. Detailed multi-scale simulation schemes have been proposed to analyze the effects of irradiation induced defects on the device electrical and optical characteristics. Nevertheless, previous works focused on residual intrinsic defects and did not include dopants [18–20]. We presented a preceding atomistic model to analyze B deactivation in irradiated Si [21], but a comprehensive understanding of the acceptor removal process is still lacking.

In this work, we address the acceptor removal process by atomistic simulations of the generation of displacement damage under neutron irradiation, and the interactions between defects and dopants. We analyze the microscopic origin of the acceptor removal mechanism, provide an explanation for the dependence of the acceptor removal constant on initial resistivity, and give some clues to identify those intrinsic defects that could act as deep acceptors.

2. Simulation scheme

We perform atomistic simulations to analyze the displacement damage resulting from neutron irradiation on *p*-type Si substrates, and its effect on the dopant profile. The energy spectrum of reactor neutrons typically spans from 10^{-8} to 10 MeV [22] but, in our simulations, we consider monoenergetic neutrons of 1 MeV as it is the standard reference for the Non-Ionizing Energy Loss (NIEL) scaling, and it is close to the NIEL weighted mean energy of the Jožef Stefan Institute (JSI) reactor (1.7 MeV) [13]. A flux of 10^{12} n cm^{-2}s^{-1} is assumed, which is in the range of those commonly used at the JSI reactor [22]. *P*-type substrate doping is simulated by considering B atoms randomly distributed, with five different concentrations ranging from 10^{13} to 10^{17} cm^{-3}. Cubic simulation cells of at least $3 \times 3 \times 3$ μm^3 are used to get enough statistics for all B concentrations. Si recoils are generated at random within the simulation volume, and periodic boundary conditions are applied in all directions to analyze the kinetics in the bulk. Irradiation is performed at RT (25 °C), covering 1-MeV neutron equivalent (n_{eq}) fluences from 10^{12} to 10^{16} cm^{-2} for a time ranging from 1 to 10^4 s, respectively. After each irradiation step the sample is annealed at 60 °C for 80 min, following the so-called CERN scenario measurement technique [23].

Several tools are combined in a multi-scale scheme so that the effects of neutron irradiation on *p*-type Si can be analyzed at an atomic level and, at the same time, macroscopic dimensions and time scales can be reached. The energy distribution of primary knock-on atoms (PKA) due to the neutron irradiation is calculated with the SPECTRA-PKA code [24] using the TENDL-2017 nuclear data library. Monoenergetic 1 MeV neutrons result in a total recoil matrix with a PKA energy spectrum that spans up to 150 keV with an average energy of 48.5 keV. Simulated neutron fluences correspond to PKA fluences from 6×10^7 to 6×10^{11} cm^{-2}, which implies that in our simulation cell and for the highest fluence more than 54,000 PKAs are simulated. Following the PKA energy spectrum, the corresponding number of recoils for each PKA energy is simulated with MARLOWE, a tool based on the binary collision approximation that provides the coordinates of the Si I's and V's [25]. The positions of Si I's and V's are transferred to the object kinetic Monte Carlo (kMC) process simulator DADOS, which only simulates the kinetics of defects and dopants during annealing and ignores the lattice [26]. In the kMC technique, system dynamics is modeled by performing random events whose probability is determined by the energetics of the defects and dopants involved in the process.

The insight gained into the mechanisms of B deactivation by implantation damage and their implementation in kMC models as the result of an extensive research on junction formation in Si devices [27], can be applied to the system analyzed in this work. However, while the fabrication of B-doped junctions often involves high local concentrations of defects and dopants and intense thermal budgets, in this study damage is diluted, B concentration is low and the annealing is reduced. Under the low thermal budget used in the aging annealing of detectors, system dynamics is governed by low activation energy events, mainly related to the diffusion of mobile species. The main interactions between defects, dopants and impurities considered in the simulations of this work are summarized in Table 1, and their energetics are provided in Tables S1–S5 in Supplementary Material. The interaction of mobile Si I's and V's is assumed to cause their mutual annihilation. When defects of the same type interact they form agglomerates of Si I's or V's (called clusters) that are mostly considered as immobile (only the di-interstitial (I_2) and tri-interstitial (I_3) defects can diffuse).

A boron-interstitial (B_i) is formed when a Si interstitial interacts with a substitutional B atom. B_i can also diffuse and interact with other defects and dopants resulting in the formation of boron-interstitial clusters. They are referred as B_nI_m, where n and m denote the number of Si I's and B atoms, respectively, and can grow in size by incorporating additional Si I's or B atoms [28]. We assume that substitutional B atoms are electrically active, contributing as shallow acceptors, while B_i and B_nI_m are considered electrically inactive and cause B deactivation. In a previous work, we explored the capabilities of our multi-scale approach to describe the damage induced by neutron irradiation, and analyzed the acceptor removal for a unique B concentration [21]. We showed that the diffusion of the I_2 and I_3 defects, which is ignored in B junction formation, plays a role on B deactivation at room or slightly elevated temperatures.

C and O impurities are incorporated in a basic model through first-order reactions. They act as traps for Si I's, V's and B_i leading to the formation of C_i, VO and B_iO defects, but higher order reactions are not included. We assume that B_iO complexes also deactivate B atoms, but they are not assigned any explicit carrier contribution. Therefore, in our code B_i, B_iO and B_nI_m are considered electrically inactive defects and they all contribute to B deactivation. Simulations were done considering 10^{17} O cm^{-3} and 2×10^{15} C cm^{-3}, in the range of impurity concentration in standard Si wafers [11,13], for all B concentrations and neutron fluences indicated above. Although more detailed models for the interactions of C and O with intrinsic defects have been proposed, for the conditions analyzed in this work our simplified model correctly describes the amount of Si I's and V's immobilized by C and

Table 1
Main equations describing defect interactions with dopants and impurities (O, C). The subscript *m* represents the number of Si I's or V's belonging to a cluster and *n* the number of B atoms in B_nI_m. Mobile species are written in bold.

$\mathbf{I} + \mathbf{V} \rightarrow 0$	$(\mathbf{I},\mathbf{I_2},\mathbf{I_3}) + B \leftrightarrow \mathbf{B_i}, BI_{(2,3)}$	$\mathbf{B_i} + I_m \leftrightarrow BI_{m+1}$
$(\mathbf{I},\mathbf{I_2},\mathbf{I_3}) + I_m \leftrightarrow I_{m+(1,2,3)}$	$\mathbf{B_i} + B \leftrightarrow B_2I$	$(\mathbf{I},\mathbf{I_2},\mathbf{I_3}) + B_nI_m \leftrightarrow B_nI_{m+(1,2,3)}$
$\mathbf{V} + V_m \leftrightarrow V_{m+1}$	$\mathbf{B_i} + \mathbf{B_i} \leftrightarrow B_2I_2$	$\mathbf{B_i} + B_nI_m \leftrightarrow B_{n+1}I_{m+1}$
$\mathbf{V} + O \leftrightarrow VO$	$C + \mathbf{I} \leftrightarrow C_i$	$\mathbf{B_i} + O \leftrightarrow B_iO$
$VO + (\mathbf{I},\mathbf{I_2},\mathbf{I_3}) \leftrightarrow O + (0,\mathbf{I},\mathbf{I_2})$	$C_i + \mathbf{V} \leftrightarrow C$	$B_iO + \mathbf{V} \leftrightarrow B + O$

O. Interstitial-rich C complexes, such as CI_2 or CI_3, are shown to be energetically unfavorable [29], and C-rich complexes are unlikely to form for the low C concentration simulated. *Ab initio* calculations suggest that O can bind to vacancy clusters leading to stable V_nO_m complexes [30]. However, this will not alter the overall number of immobilized vacancies, as V's clusters are already stable for the temperature range of our simulations.

As a benchmark for our model, we compare the experimental introduction rates for VO derived from DLTS with those in our simulations. Depending on experimental conditions, introduction rates of 0.1, 0.63 and 3.4 cm^{-1} have been reported [31–33], usually for low fluence irradiation. In our simulations with O and C (10^{15} B cm^{-3}, 10^{17} O cm^{-3}, 2×10^{15} C cm^{-3}) irradiated with 10^{12} n_{eq} cm^{-2} we obtain a VO concentration of 1.3 × 10^{12} cm^{-3}, which corresponds to an introduction rate of ~1.3 cm^{-1}. This value is consistent with experimental results, although the amount of VO in simulations may be overestimated, as some of them may evolve to higher order V_nO_m complexes that are not considered in our model.

Unlike empirical models that use first order equations for defect-dopant reactions and fitting parameters for the amount of displacement damage and the probability of defect-dopant interactions, in our simulation scheme, the amount, distribution and topology of damage and defect-dopant interactions are naturally derived from atomistic simulations, with no previous assumptions. Our model takes into account the complex interactions between Si I's and B atoms, including higher order reactions, which allows a detailed analysis of B deactivation processes. However, our simulation scheme has some limitations. The kMC simulator does not explicitly include the charge state of dopants and defects. For the discussion on the electrical activity of defects we assume those states obtained by *ab initio* calculations reported in literature. Impurities (C, O) are described with a simplified model that captures their role as traps but not the complex scenario that may arise from the interactions between intrinsic defects, dopants and impurities (C_nI_m, V_nO_m, C-O, B-O, B-C complexes).

3. Results and discussion

We have analyzed the acceptor removal process by simulating B deactivation under neutron irradiation. We use experimental data available in literature [7,8,34] and our own experimental results for a radiation-hard power switch described elsewhere [21,35] to validate our model [21]. Estimated N_{eff} values from the measured drain currents in our switch, along with other experimental N_{eff} obtained from V_{FD} measurements of irradiated devices [7,8,34] are plotted in Fig. 1. At first, N_{eff} significantly reduces with fluence, but at high fluences a linear increase is observed. This increase has been associated with the contribution to space charge of electrically active defects, which have a net acceptor behavior, increasing V_{FD}. The evolution of the experimental N_{eff} in our switch is slightly different. It presents a small plateau at low fluences, then a steeper decay with fluence and a final saturation at high fluences, but no increase is observed. In our case, N_{eff} is not derived from V_{FD} measurements that detect the amount of space charge, but from bulk

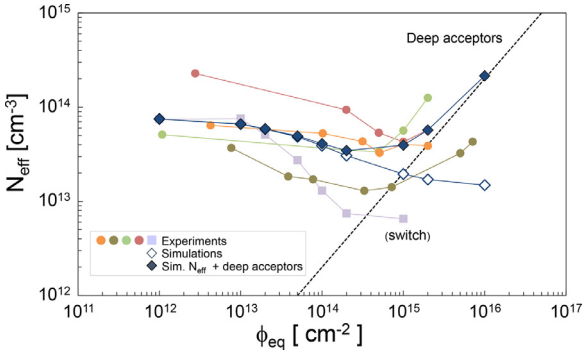

Fig. 1. Experimental and simulated N_{eff} as a function of 1-MeV n_{eq} fluence for $N_{eff,0}$ in the range of 10^{14} B cm^{-3}. Experimental N_{eff} was extracted from full depletion voltage (V_{FD}) (circles) [7,8,34] and resistivity (squares) [21] measurements. The dashed line represents the formation of deep acceptors estimated from the experimental introduction rate of 0.02 cm^{-1}. Simulation results correspond to N_{eff} (open diamonds) and N_{eff} plus the deep acceptor concentration calculated as 0.02 cm^{-1} × ϕ_{eq} (solid diamonds).

resistivity values, which is actually a measure of the concentration of free carriers. At low fluences, the concentration of free carriers equals the space charge concentration (since space charge is mostly due to ionized dopants), but at high fluences the contribution of electrical active defects to space charge exceeds that of dopants. The simulated N_{eff} (open diamonds in Fig. 1) corresponds to the concentration of substitutional B atoms, i.e. B atoms that are still active and can contribute as acceptors. At low fluences, our simulated data follow the same trend as experimental N_{eff} values. To get a global picture of the evolution of N_{eff} with fluence, we have added to the simulated N_{eff} values the contribution of deep acceptors (dashed line) (calculated as the experimental introduction rate 0.02 cm^{-1} × fluence [10,11]). The resulting N_{eff} curve (plotted as solid diamonds) provides a consistent description of the process in the whole fluence range.

The dependence of N_{eff} on fluence is usually parametrized following the so-called "Hamburg model" [36] as

$$N_{eff}(\phi_{eq}) = N_{eff,0} - N_C(\phi_{eq}) + g_c\phi_{eq} \quad with$$
$$N_C(\phi_{eq}) = N_{C,0}\left[1 - \exp\left(-c_A\phi_{eq}\right)\right] \qquad (1)$$

where ϕ_{eq} is the 1-MeV NIEL equivalent fluence, $N_{eff,0}$ the initial acceptor concentration, N_C and $N_{C,0}$ the concentration of removed acceptors and removable acceptors ($N_{C,0} \leq N_{eff,0}$), respectively, c_A the acceptor removal constant, and g_c the introduction rate of stable defect-related deep acceptors. The Hamburg model takes into account both the sharp reduction of N_{eff} with fluence at low fluences, and its linear raise at higher fluences. The acceptor removal process can be better analyzed by defining the parameter ϕ_A as the inverse of the removal constant ($\phi_A = 1/c_A$). ϕ_A represents the fluence at which N_C has reached 63% of its final value ($N_{C,0}$) and identifies the steep-decay region in N_{eff} curves. It can be envisioned as a figure of merit of the detector radiation hardness as it refers to the fluence that the detector can endure before significant dopant deactivation occurs. In the following sections, we present simu-

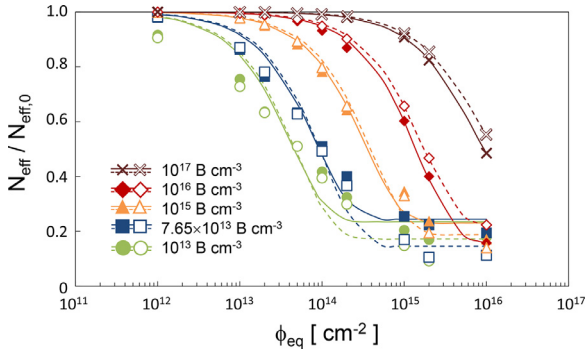

Fig. 2. Simulated $N_{eff}/N_{eff,0}$ as a function 1 -MeV n_{eq} fluence for $N_{eff,0}$ from 10^{13} to 10^{17} B cm^{-3}. Lines show the fitting of data to Eq. (1). Solid symbols and lines correspond to simulations with no impurities, while open symbols and dashed lines represent simulations with 10^{17} O cm^{-3} and 2 × 10^{15} C cm^{-3}.

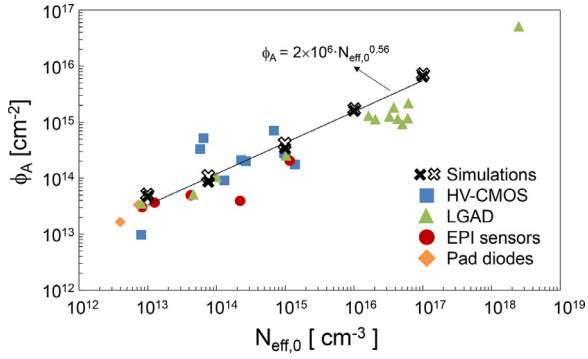

Fig. 3. Acceptor removal parameter ϕ_A as a function of $N_{eff,0}$. Simulation results with no impurities are plotted as solid crosses and fitted to a power equation (solid line), while open crosses correspond to simulations with 10^{17} O cm^{-3} and 2 × 10^{15} C cm^{-3}. Solid symbols show experimental data from literature for HV-CMOS sensors [6–9,38,39], LGAD [3,37], sensors made from EPI Si [34,37] and Pad diodes [39].

lations of acceptor removal under neutron irradiation for a wide range of substrate resistivities. We use experimental data from literature to analyze the physical mechanisms that explain the values of ϕ_A and g_c, and the dependence of ϕ_A on $N_{eff,0}$, as these are the key parameters that determine the evolution of N_{eff} with fluence.

3.1. Acceptor removal parameter ϕ_A

The acceptor removal constant c_A has been systematically reported to decrease with $N_{eff,0}$ (i.e. ϕ_A increases with $N_{eff,0}$) [3–5,9,37]. To analyze this dependence, we have performed a total number of 90 simulations, including 9 neutron fluences and 5 $N_{eff,0}$ values, with and without impurities (O, C). Dopant concentration ranges between 10^{13} and 10^{17} B cm^{-3}, covering the high- and low-resistivity substrates of standard Si sensors and novel detectors (LGAD, HV-CMOS), respectively. In Fig. 2 we show the simulated relative effective dopant concentration, i.e. the ratio $N_{eff}/N_{eff,0}$, as a function of 1-MeV n_{eq} fluence for the doping range mentioned before. Our results reveal that as $N_{eff,0}$ increases the sharp decay region is shifted to larger fluences, consistently with experimental observations. For instance, for 10^{13} B cm^{-3} N_{eff} is reduced to a 50% of its original value after a fluence of 5 × 10^{13} n_{eq} cm^{-2}, while for 10^{17} B cm^{-3} a fluence of 10^{16} n_{eq} cm^{-2} is required to achieve the same reduction in $N_{eff}/N_{eff,0}$. Simulated N_{eff} curves are fitted to Eq. (1) using $N_{C,0}$ and ϕ_A as fitting parameters (solid lines in Fig. 2). The extracted values of ϕ_A as a function of $N_{eff,0}$ are compared in Fig. 3 to those obtained from the experimental removal constants c_A ($\phi_A = 1/c_A$) available in literature. Experimental data correspond to the analysis of N_{eff} obtained from V_{FD} measurements, and include different detector architectures as HV-CMOS sensors [6–9,38,39], LGAD [3,37], sensors made from EPI Si [34,37] and Pad diodes [39]. ϕ_A values obtained from simulations are comparable to the experimental ones and follow a sublinear trend with $N_{eff,0}$ according to equation $\phi_A = 2 \times 10^6\ {N_{eff,0}}^{0.56}$ cm^{-2}.

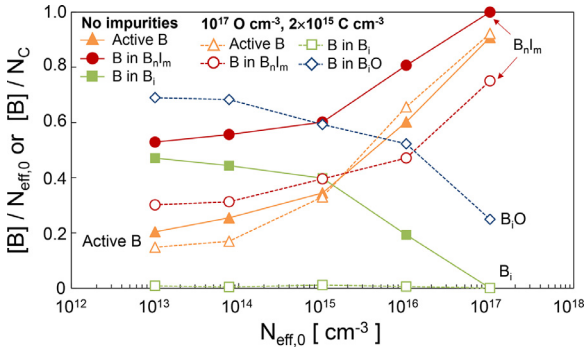

Fig. 4. Simulated fraction of active B ([B]/$N_{eff,0}$) (triangles), and fraction of deactivated B ([B]/N_C) in B_nI_m (circles), B_i (squares) and B_iO complexes (diamonds) after 10^{15} n_{eq} cm^{-2} as a function of $N_{eff,0}$. Simulations were done without impurities (solid symbols), and with 10^{17} O cm^{-3} and 2×10^{15} C cm^{-3} (open symbols).

3.2. Role of O and C on acceptor removal

The presence of O and C in Si wafers in concentrations comparable or higher than $N_{eff,0}$ [11,13] may play a role on acceptor removal since they interact with defects and dopants. It is well established that the existence of O leads to the formation of VO and higher order V-O complexes by capturing V's [40], while C atoms react mainly with Si I's via the formation of C_i and C-I complexes [41]. Several studies indicate that B_i has a strong affinity for pairing with O, resulting in B_iO complexes [42,43]. Traditionally, B_iO is assumed to behave as a donor in the upper part of the Si bandgap and is assigned a key role on acceptor removal [42,43]. However, recent studies attribute tentatively this donor level to B-I defects [44], and the large scattering of B_iO electrical characterization suggests a more complex scenario in which higher order defects involving B, O and Si I's may exist [45]. To analyze the role of impurities on the removal process new simulations were done assuming 10^{17} O cm^{-3} and 2×10^{15} C cm^{-3}, consistent with impurity concentrations in standard Si substrates. The resulting $N_{eff}/N_{eff,0}$ and ϕ_A values are also depicted in Fig. 2 and Fig. 3 (open symbols), respectively. The introduction of these concentrations of O and C has a small effect on the amount of removed acceptors, and simulations with and without impurities lead to similar removal parameters.

In order to elucidate B deactivation mechanisms, we have quantified in Fig. 4 the fraction of B ([B]/$N_{eff,0}$) that remains substitutional (i.e. active B), in samples with and without impurities after 10^{15} n_{eq} cm^{-2}. We also show the relative weight on the total amount of deactivated B ([B]/N_C) of B_i, B_nI_m and B_iO complexes. For low $N_{eff,0}$, in the sample without impurities, deactivated B is almost equally distributed between B_i and B_nI_m. However, in the sample with O and C, most deactivated B belongs to B_iO complexes, the amount of B_nI_m has notably reduced and there is almost no B_i. At high $N_{eff,0}$, the large amount of B atoms enhances B_nI_m formation becoming the main mechanism of acceptor removal in both samples.

A detailed analysis of our simulations indicates that in the sample without O and C, B deactivation starts with the formation of B_i and small B_nI_m (BI_2, BI_3) through the interaction of mobile Si I's defects (I, I_2, I_3) with B (see Table 1). As $N_{eff,0}$ increases, diffusing B_i defects are likely to interact with other B atoms (substitutional B, B_i, B_nI_m). Thus, the fraction of B in B_nI_m increases at the expense of B_i. In the presence of O and C, for low $N_{eff,0}$,

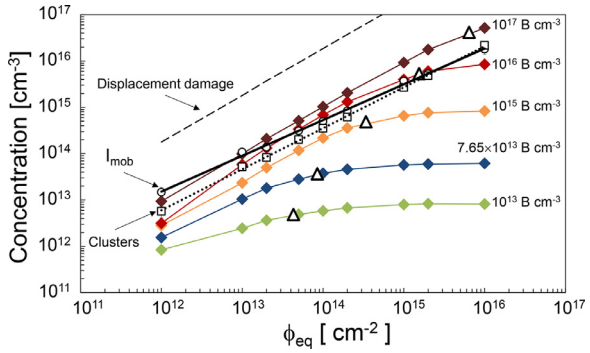

Fig. 5. Simulated concentration of removed acceptors (diamonds) as a function of 1 MeV n_{eq} fluence, for $N_{eff,0}$ from 10^{13} to 10^{17} B cm^{-3}. Triangles show the removal parameter ϕ_A obtained for each $N_{eff,0}$. The concentration of generated damage is plotted as a dashed line, and the concentration of I_{mob} and defect clusters after irradiation as circles and squares, respectively, while solid and dotted lines are the best fit to a power equation.

oxygen concentration is significantly higher than that of B, which enhances the interaction of B_i with O forming immobile B_iO complexes. This notably reduces B_i population and limits the growth path for larger B_nI_m, as in our model the interaction of Si I's or B_i with B_iO complexes is not considered. Besides, a high concentration of VO defects is also formed that can annihilate mobile Si I's (I_{mob}), hindering the formation of small B_nI_m through the diffusion of I_2 and I_3. Regarding C atoms, their main role is the trapping of Si I's in C_i reducing B diffusion and clustering [3]. However, in our sample the effect of C is mitigated by the relatively low C concentration and a much higher O concentration (usual in standard Si wafers). As many V's are immobilized at VO defects, I-V annihilation is reduced. This increases the amount of available mobile Si I's and compensates the trapping of Si I's in C_i. Therefore, the presence of O and C results in different complexes that deactivate B atoms, reducing the concentration of B_i and B_nI_m in favor of B_iO complexes for high O concentrations. However, for the conditions analyzed ([O] >> [C]) and within the simplified model used in this work, O and C have little effect on the overall amount of substitutional B atoms, electrically active in the model. For this reason, the analysis of acceptor removal in the following sections is based on simulations with no impurities, although the effect of O and C will be occasionally addressed.

3.3. Dependence of removal parameter on substrate resistivity

Experimental and simulated results reported in Fig. 3 show that as $N_{eff,0}$ increases larger neutron fluences (higher values of ϕ_A) are required to deactivate the dopants. Previous attempts to explain the acceptor removal process based on defect kinetics did not provide a fully satisfactory description of experimental data [14,15], and this dependence stills remains a riddle. In order to shed light on this issue we have studied the atomistic mechanisms behind dopant deactivation.

From our simulations, we analyze the damage resulting from 1 MeV neutron irradiation and the effect of $N_{eff,0}$ and fluence on the deactivation process. In Fig. 5 we show the concentration of displacement damage (Si I's and V's) generated in irradiation cascades (dashed line) as provided by Marlowe before any annealing is done. The concentration of I_{mob} (circles and solid line) and Si I's and V's clusters (squares and dotted line) as a function of fluence is also plotted. I_{mob} and cluster concentrations are computed after irradiation steps and are averaged values from simulations with 10^{13} to 10^{17} B cm^{-3}, although standard deviation (error bars in the figure) is negligible. The generated displacement damage increases linearly with fluence as it is only determined by the number and energy of PKAs. The great difference between the number of generated defects and those remaining (I_{mob} or clusters) is a clear indication that during RT irradiation intense I-V annihilation has occurred. The amount of I_{mob} and clusters is similar and both increase sublinearly with fluence ($[I_{mob}] = 8227\phi_{eq}^{0.77}$ cm^{-3}; [Clusters] = $145\ \phi_{eq}^{0.88}$ cm^{-3}) due to an enhanced annihilation at high fluences as generated defects are in close proximity. The concentration of removed acceptors N_C (diamonds) and the acceptor removal parameter ϕ_A obtained for each $N_{eff,0}$ (open triangles) are also plotted in the figure. We can see that N_C initially increases with fluence but it saturates at high fluences when most dopants have already been deactivated (as reported in Fig. 2). The saturation onset is shifted to higher fluences as $N_{eff,0}$ increases and is consistent with the extracted ϕ_A values.

The acceptor removal is caused by the interaction of I_{mob} with substitutional B atoms but V's and Si I's clusters formed along the cascade can annihilate or trap I_{mob}, respectively, hindering them from reaching B atoms. Consequently, the efficiency of the removal process relies on two parameters: the concentration of mobile Si I's remaining after irradiation ($[I_{mob}]$), and the probability of these Si I's interacting with B atoms ($\rho_{I\text{-}B}$), instead of being annihilated or trapped. Thus, we can estimate the amount of Si I's that can effectively reach and potentially deactivate B atoms ("effective" mobile Si I's, $I_{mob,eff}$) as indicated in Eq. (2). The probability $\rho_{I\text{-}B}$ is calculated as the ratio of the dopant concentration to the total concentration of traps for Si I's (dopants, V's (V_{cl}) and Si I's (I_{cl}) clusters) according to Eq. (3).

$$\left[I_{mob,eff}\right] \approx [I_{mob}]\rho_{I-B} \tag{2}$$

$$\rho_{I-B} \approx \frac{[B]}{[B] + [V_{cl}] + [I_{cl}]} \tag{3}$$

At low fluences and high $N_{eff,0}$ the amount of B atoms notably exceeds that of annihilating or trapping defects ([B] >> [V_{cl} + I_{cl}]) and $\rho_{I\text{-}B}$ approaches unity. Consequently, the number of $I_{mob,eff}$, and therefore the amount of B that can be potentially deactivated, is determined by the number of available mobile Si I's ($N_C \sim I_{mob,eff} \sim I_{mob}$). This corresponds in our simulations (Fig. 5) to the region where N_C curves (for different $N_{eff,0}$) grow with fluence with a similar slope as I_{mob}, and the values of N_C and I_{mob} are comparable. In this regime, the number of I_{mob} is low due to the intense intracascade I-V annihilation, and dopant deactivation is limited by the availability of diffusing Si I's. On the contrary, at large fluences and low $N_{eff,0}$, the amount of defect clusters is much larger than that of B ([B] << [V_{cl} + I_{cl}]) and $\rho_{I\text{-}B} \sim [B]/[V_{cl} + I_{cl}]$ according to Eq. (3). Since the population of I_{mob} and defect clusters is similar ([V_{cl} + I_{cl}] ~ I_{mob}), the number of $I_{mob,eff}$ that deactivate B atoms becomes proportional to B concentration ($N_C \sim I_{mob,eff} \propto [B]$). This corresponds to the saturated region in Fig. 5 in which N_C is described by horizontal lines whose value is determined by $N_{eff,0}$. In this situation, there are enough I_{mob} but the presence of a large amount of defect clusters reduces the probability of their interaction with B. The onset of the saturation regime occurs when the amount of I_{mob} and defect clusters is comparable to that of B ([B] ~ I_{mob} ~ [V_{cl} + I_{cl}]). The acceptor removal parameter ϕ_A can be regarded as the fluence required to produce a number of I_{mob} similar to $N_{eff,0}$, resulting in significant dopant deactivation and the onset of saturation. Thus, ϕ_A increases with $N_{eff,0}$ because more I_{mob} are required to deactivate the dopants.

In Fig. 5 we observe some deviation from the previous simplified description. On one hand, for low fluences and dopant concentrations, N_C lies below the I_{mob} line and the curves approach I_{mob} as $N_{eff,0}$ increases. This is mainly due to the inhomogeneity of neutron irradiation damage: defects are close to each other along the cascade trajectory but there is a large distance between neighboring cascades, especially at low fluences. Within 50 keV recoils,

each defect (Si interstitial or vacancy) has on average 4.6 neighboring defects within a radius of 2 nm, which is much shorter than the mean inter-cascade distance (403 nm for 10^{13} n cm^{-2} corresponding to a PKA fluence of 6×10^{8} cm^{-2}). As a result, intracascade defect annihilation and clustering is favored, compared to what it would be obtained if the same V's and Si I's concentration were homogeneously distributed [46]. It reduces the actual probability of I_{mob} reaching B atoms and, therefore, the efficiency of the removal process. This effect is made up by increasing the amount of I_{mob} required to deactivate the dopants, which shifts ϕ_A to higher fluences than expected. On the other hand, at high fluences and dopant concentrations N_C values slightly exceed the number of I_{mob}. It indicates the existence of more efficient deactivation mechanisms in which each I_{mob} can deactivate several B atoms ($I + B \rightarrow B_i$; $B_i + B \rightarrow B_2I$). In this case, the high B concentration favors the formation of B_nI_m with more than one B atom which boosts the removal process. This mechanism reduces the number of required I_{mob} and shifts ϕ_A to lower fluences. As a consequence, although ϕ_A was expected to follow a similar trend as I_{mob}, the inhomogeneity of damage at low fluences and the formation of B-rich B_nI_m at high $N_{eff,0}$ result in the sublinear dependence of ϕ_A on $N_{eff,0}$ obtained in our atomistic simulations and reported in the experiments gathered in Fig. 3.

Although the overall effect of the simulated concentrations of O and C (when [O] >> [C]) on acceptor removal is limited, they are responsible for slight modifications on defect dynamics. In our simulated samples enriched with O and C, the formation of VO and C_i by trapping some V's and Si I's initially prevents them from annihilating and increases the amount of mobile V's and Si I's after irradiation. However, during annealing VO and C atoms can annihilate or trap I_{mob}, limiting its probability of interacting with B. These two effects compensate to a large extent since there are initially more I_{mob} but they are more likely to annihilate in a later stage. It explains why in our model, and for the impurity concentrations used in this work, the amount of deactived B is hardly affected by the presence of O and C.

3.4. Microscopic origin of deep acceptors

Experiments reveal that at large irradiation fluences N_{eff} increases almost linearly with fluence, following an acceptor generation rate of $g_c \sim 0.02$ cm^{-1} [10,11], as indicated in Eq. (1). N_{eff} may even exceed $N_{eff,0}$, which suggests that other defects in addition to dopants are contributing with negative space charge. Besides, similar values of g_c have been reported under neutron irradiation independently of substrate resistivity, in both *p*- and *n*-type substrates, and for materials with different O contents [47]. Consequently, the increase of N_{eff} with fluence has been attributed to the formation of radiation-induced electrically active intrinsic defects, with a joint contribution of several donor and deep acceptor levels, the latter ones being predominant [12,13]. This supports the idea that in neutron-irradiated *p*-type Si N_{eff} is determined by two competing mechanisms: an initial acceptor removal at low and medium fluences caused by B deactivation by Si I's, and the formation of deep acceptors at large fluences associated to the accumulation of intrinsic defects. Extensive research has been devoted to identify the defects most plausible candidates to behave as deep acceptors. Defects proposed from experimental and theoretical studies are in general vacancy-like, and include small vacancy defects or oxygen-related defects [33,48], clustered or extended defects [12,13] and small amorphous regions [49]. The linking between microscopic defects and macroscopic effects is difficult because a large variety of irradiation-induced defects with different sizes and configurations simultaneously coexists, and they may even contain dopants and impurities. We combine the information obtained from the experimental characterization, *ab initio* calculations and our kMC simulations to get insight into the main contributors to N_{eff} as deep acceptors.

Experimental defect characterization relies on the use of different irradiation particles to bias damage towards the predominance of point defects or clusters, the controlled introduction of impurities (mainly C and O), and the annealing of irradiated samples to determine the thermal stability of defects. DLTS and TSC techniques characterize electrically active defects, providing parameters such as the associated energy level in the Si bandgap, the donor- or acceptor-like behavior, the capture cross-section for carriers and the estimated concentration. However, the identification of specific defects responsible for the peaks of the DLTS/TSC spectrum is not straightforward. Three main acceptor levels were detected, labeled as H116K, H140K y H152K, with energy levels in the lower part of the Si bandgap and a generation rate of ~ 0.04 cm^{-1} [13]. These acceptor levels were associated to bistable defect clusters, presenting two configurations with different electrical activity. As their behavior resembled that of small V's clusters these levels were tentatively attributed to clusters with more than 3 V's [12].

Ab initio simulations allow the characterization of small defect clusters with a previously defined configuration, providing their formation energy and the energy levels introduced in the Si bandgap. Nevertheless, the underestimation of the Si bandgap results in some uncertainty on the calculated energy levels [50], and the high computational cost limits the electrical behavior studies to small sizes: up to the tetra-interstitial and the hexa-vacancy. Usually, donor levels are obtained for Si I's clusters [51,52], and acceptors levels in the upper part of the Si bandgap (some close to mid-gap) for V's clusters [50]. To our knowledge, there is no theoretical evidence of specific defects with deep acceptor levels consistent with those of H116K, H140K and H152K peaks. The energy levels of small V's clusters derived from *ab initio* calculations are compiled in Table 2 [50,53,54]. Vacancy clusters larger than V_2 are known to be bistable defects existing in two configurations: Part-of-Hexagonal-Ring (PHR) and Four-Fold Coordinated (FFC), FFC being the most stable one [50]. For V_3 both configurations have been observed: PHR V_3 is detected at RT, while FFC V_3 is formed after annealing and presents an acceptor level at 75 meV below conduction band edge (E_c) [54]. The deepest acceptor levels for V's clusters reported from *ab initio* calculations are 0.46 eV (PHR $V_3^{-/0}$), 0.54 eV (FFC $V_4^{=/-}$ and $V_4^{-/0}$), 0.47 eV (FFC $V_5^{=/-}$) and 0.45 eV (FFC $V_5^{-/0}$) below E_c. Note that an acceptor level at E_c - 0.7 eV was obtained for PHR $V_4^{-/0}$ in Ref. [50], which lies within the lower part of the bandgap, but the authors point out that it may be overestimated in their calculations.

Our kMC simulations provide the concentration and size distribution of Si I's and V's clusters as the result of defects diffusion and interactions in neutron-irradiated *p*-type Si. Electrically active defects that can significantly contribute to N_{eff} should be present in a concentration similar or higher than that corresponding to the experimental factor g_c. In Fig. 6 we report the concentration versus fluence of the most abundant V's and Si I's clusters in a simulation with $N_{eff,0} = 10^{15}$ B cm^{-3}, and the corresponding fitted power equations as dashed lines (fitting parameters are compiled in Table S6 and Fig. S1 in Supplementary Material). The solid black line corresponds to the effective deep acceptor concentration estimated from the experimental generation rate $g_c \sim 0.02$ cm^{-1}. It represents the net contribution of donor and deep acceptor levels, while a higher introduction rate of ~ 0.04 cm^{-1} was obtained for the main acceptor levels reported in DLTS/TSC [13]. The figure shows that small clusters are predominant and as cluster size increases their concentration is notably reduced. To estimate whether the amount of clusters we get agrees with experiments, we compare our simulation results against the V_2 concentration obtained from DLTS measurements. Introduction rates of 4.7 cm^{-1} for V_2 [33], and 0.3 and 1.4 cm^{-1} for $V_2^{(=,-)}$ and $V_2^{(-,0)}$, respectively [55], have

Table 2
Energy level (E, below the conduction band edge), occupancy (η) and associated introduction rate of negative space charge (g_{cl}) of small vacancy clusters considering $\sigma_e = 2 \times 10^{-15}$ cm^2 and σ_h/σ_e ratios of 10 and 100. Energy levels are extracted from *ab initio* calculations available in literature [50,53,54]. η lower than 0.01% and g_{cl} lower than 0.001 cm^{-1} are denoted by "–".

		$V_2^{=/-}$	$V_2^{-/0}$	$V_3^{=/-}$(PHR)	$V_3^{-/0}$(PHR)	$V_4^{=/-}$(FFC)	$V_4^{-/0}$(FFC)	$V_5^{=/-}$(FFC)	$V_5^{-/0}$(FFC)	$V_6^{-/0}$(FFC)
E_c - E (eV)		0.23	0.42	0.36	0.46	0.54	0.54	0.47	0.45	0.36
$\sigma_h/\sigma_e = 10$	η (%)	–	0.02	–	0.34	50.98	30.63	–	0.16	–
	g_{cl} (cm^{-1})	–	–	–	0.002	0.229	0.069	–	–	–
$\sigma_h/\sigma_e =$	η (%)	–	0.15	–	3.30	94.01	5.65	0.11	1.55	–
100	g_{cl} (cm^{-1})	–	0.001	–	0.016	0.422	0.013	–	0.010	–

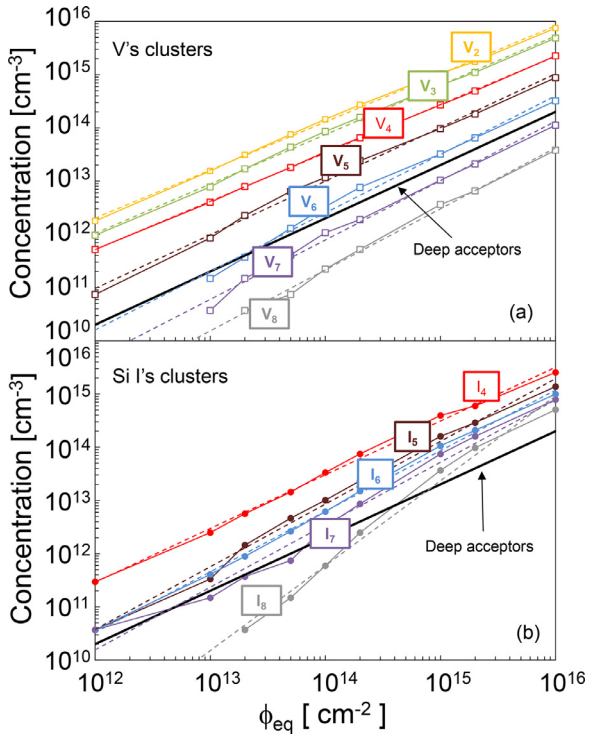

Fig. 6. Simulated concentration of V's (a) and Si I's (b) clusters with different sizes as a function of 1 MeV n_{eq} fluence in a simulation with $N_{eff,0} = 10^{15}$ B cm^{-3}. Dashed lines show the fitting of cluster concentrations to power equations, and black solid lines the deep acceptor concentration estimated from the experimental generation rate.

been reported. The V_2 concentration shown in Fig. 6 after 10^{12} n cm^{-2} is 1.8×10^{12} cm^{-3}, which corresponds to an introduction rate of 1.8 cm^{-1}, in the order of those derived from DLTS at low irradiation fluences. According to our simulations, only small clusters with a size up to 5-6 defects are abundant enough compared to the deep acceptor concentration deduced from the experimental generation rates.

Intrinsic defects that play a major role on the increase of N_{eff} with fluence must exist in a concentration high enough, and have acceptor energy levels in the lower part of the bandgap or close to mid-gap to have a significant occupancy. We estimate the contribution of an electrically active defect to N_{eff} from the concentration obtained by kMC simulations and its steady-state occupancy. This is calculated from the Shockley-Read-Hall statistics as done in Ref. [13], assuming full depletion (zero free carriers). We use energy levels in the bandgap reported by *ab initio* calculations and electron (σ_e) and hole (σ_h) capture cross sections derived from DLTS/TSC. For acceptors in the upper part of the bandgap, σ_e in the order of 2–4 $\times 10^{-15}$ cm^2 has been reported [12]. Continuum models use σ_h as a fitting parameter assuming $\sigma_h/\sigma_e \approx 10$ [16] as few experimental values are known (only $\sigma_h/\sigma_e \approx 100$ for PHR $V_3^{-/0}$) [12]. In Table 2 we show the energy levels (E, below E_c) reported in literature for small vacancy clusters (V_2-V_6) with different charge states, and the calculated occupancy (η) assuming $\sigma_e = 2 \times 10^{-15}$ cm^2 and using two different σ_h/σ_e ratios of 10 and 100. For each cluster size, the total defect concentration is distributed among the different charge states including the neutral state (not shown in Table 2). FFC V_4 clusters show a high occupancy as their energy levels are close to mid-gap (E_c - 0.54 eV). Considering cluster concentrations reported in Fig. 6 and the obtained occupancy, we determine the introduction rate of negative space charge associated to each cluster (g_{cl}) (singly and doubly charged defects contribute with one or two charges to N_{eff}, respectively). Our results indicate that, in full depletion, the contribution of FFC $V_4^{=/-}$ is dominant and we even overestimate the increase of N_{eff} with irradiation fluence. Other small V's clusters (FFC $V_4^{-/0}$, PHR $V_3^{-/0}$, and FFC $V_5^{-/0}$) contribute to a lower extent and some compensation with donor-like defects may also occur. Although we have not found a correspondence with the acceptor levels H116K, H140K, H152K measured by DLTS/TSC, our analysis is consistent with empirical radiation damage models of irradiated *p*-type sensors, which require acceptor levels in the range of 0.42–0.52 eV below E_c (similar to the energy levels of V_3, V_4, V_5 clusters) to fit their experimental electrical behavior [37].

4. Conclusions

We present the first TCAD study that addresses the acceptor removal process in neutron-irradiated *p*-type Si by means of atomistic simulations of defect-dopant interactions. The acceptor removal can be successfully modeled by simulating B deactivation induced by Si I's generated by irradiation. We combine several simulation techniques to describe neutron irradiation damage and dopant deactivation processes without specific fitting parameters or previous assumptions. Our defect-dopant atomistic model, widely tested in Si process simulation, is extended to include I_2 and I_3 as mobile defects as they play a key role on B deactivation under the operational conditions of particle detectors.

From the analysis of N_{eff} on a wide range of $N_{eff,0}$ (10^{13}–10^{17} B cm^{-3}) we obtain acceptor removal parameters that are consistent with those experimentally reported and with the same dependence on substrate resistivity. Our study reveals that the efficiency of the acceptor removal process strongly depends on the relative population of I_{mob}, defect clusters and B atoms. We show that the increase of the acceptor removal parameter ϕ_A with $N_{eff,0}$ is due to the limited amount of I_{mob} at low fluences and the reduced probability of I-B interaction as fluence increases. The shortage of I_{mob} is caused by intense I-V annihilation within irradiation cascades, and by the trapping of Si I's in clusters that prevents them from interacting with dopants. Defect clusters play a key role by annihilating and trapping I_{mob} since, contrary to impurities and other traps for Si I's whose number remains constant during irradiation, cluster concentration increases with fluence and may even exceeds that of I_{mob}. To provide a detailed description of the acceptor removal mechanism, B deactivation models must consider the inhomogene-

ity of neutron irradiation damage (especially relevant at low fluences) and the formation of B_nI_m at high $N_{eff,0}$ through higher order reactions between defects and dopants (at least $B_i + B \leftrightarrow B_2I$). These mechanisms are responsible for the sublinear dependence of ϕ_A on $N_{eff,0,}$ since they affect the efficiency of the removal process and therefore the amount of I_{mob} required to deactivate the dopants. We have analyzed the role of O and C on acceptor removal by including for the formation of VO, C_i and B_iO defects in our model. The presence of O and C modifies B deactivation mechanisms due to the key role of B_iO defects and the trapping of intrinsic defects by O and C. However, for the impurity concentrations used in this work ([O] >> [C]), it has little effect on the overall amount of removed acceptors.

We provide a comprehensive description of N_{eff} for the overall neutron fluences commonly used in high energy physics, by identifying the mechanisms of B deactivation and the simultaneous generation of defect clusters. The analysis at an atomistic level of defect cluster population, combined with the energy levels provided by *ab initio* and the insight of DLTS/TSC characterization, leads us to propose that the FFC V_4 significantly contributes to N_{eff} at high neutron irradiation fluences.

Declaration of Competing Interest

The authors declare that they have no known competing financial interests or personal relationships that could have appeared to influence the work reported in this paper.

Acknowledgments

This work has been supported by the Spanish Ministerio de Ciencia e Innovación under Project No. PID2020-115118GB-I00 and PID2019-110189RB-C22. The authors would like to thank Dr. P. Castrillo for his contribution on the calculation of defect levels occupancy.

Supplementary materials

Supplementary material associated with this article can be found, in the online version, at doi:10.1016/j.actamat.2022.118375.

References

[1] W. Adam, et al., *P*-type silicon strip sensors for the new CMS tracker at HL-LHC, J. Instrum. 12 (2017) P06018.
[2] R. Wunstorf, W.M. Bugg, J. Walter, F.W. Garber, D. Larson, Investigations of donor and acceptor removal and long term annealing in Si with different boron/phosphorous ratios, Nucl. Instrum. Methods Phys. Res. A 377 (1996) 228–233.
[3] M. Ferrero, et al., Radiation resistant LGAD design, Nucl. Instrum. Methods Phys. Res. A 919 (2019) 16–26.
[4] G. Kramberger, M. Baselga, V. Cindro, P. Fernandez-Martinez, D. Flores, Z. Galloway, A. Gorišek, V. Greco, S. Hidalgo, V. Fadeyev, I. Mandić, M. Mikuž, D. Quirion, G. Pellegrini, H.F-W. Sadrozinski, A. Studen, M. Zavrtanik, Radiation effects in low gain avalanche detectors after hadron irradiations, J. Instrum. 10 (2015) P07006.
[5] G. Kramberger, M. Carulla, E. Cavallaro, V. Cindro, D. Flores, Z. Galloway, S. Grinstein, S. Hidalgo, V. Fadeyev, J. Lange, I. Mandić, G. Medin, A. Merlos, F. McKinney-Martinez, M. Mikuž, D. Quirion, G. Pellegrini, M. Petek, H.F.-W. Sadrozinski, A. Seiden, M. Zavrtanik, Radiation hardness of thin low gain avalanche detectors, Nucl. Inst. Methods Phys. Res. A 891 (2018) 68–77.
[6] A. Affolder, et al., Charge collection studies in irradiated HV-CMOS particle detectors, J. Instrum. 11 (2016) P04007.
[7] E. Cavallaro, R. Casanova, F. Förster, S. Grinstein, J. Lange, G. Kramberger, I. Mandić, C. Puigdengoles, S. Terzo, Studies of irradiated AMS H35 CMOS detectors for the atlas tracker upgrade, J. Instrum. 12 (2017) C01074.
[8] B. Hiti, et al., Charge collection in irradiated HV-CMOS detectors, Nucl. Instrum. Methods Phys. Res. A 924 (2019) 214–218.
[9] I. Mandic, V. Cindro, A. Gorišek, B. Hiti, G. Kramberger, M. Mikuž, M. Zavrtanik, T. Hemperek, M. Daas, F. Hügging, H. Krüger, D.-L. Pohl, N. Wermes, L. Gonella, Neutron irradiation test of depleted CMOS pixel detector prototypes, J. Instrum. 12 (2017) P02021.
[10] V. Cindro, G. Kramberger, M. Lozano, I. Mandic, M. Mikuž, G. Pellegrini, J. Pulko, M. Ullan, M. Zavrtanik, Radiation damage in *p*-type silicon irradiated with neutrons and protons, Nucl. Instrum. Methods Phys. Res. A 599 (2009) 60–65.
[11] G. Lindström, et al., Radiation hard silicon detectors—developments by the RD48 (ROSE) collaboration, Nucl. Instrum. Methods Phys. Res. A 466 (2001) 308–326.
[12] R. Radu, I. Pintilie, L.C. Nistor, E. Fretwurst, G. Lindstroem, L.F. Makarenko, Investigation of point and extended defects in electron irradiated silicon-Dependence on the particle energy, J. Appl. Phys. 117 (2015) 164503.
[13] I. Pintilie, G. Lindstroem, A. Junkes, E. Fretwurst, Radiation-induced point- and cluster-related defects with strong impact on damage properties of silicon detectors, Nucl. Instrum. Methods Phys. Res. A 611 (2009) 52–68.
[14] M. Centis, Acceptor removal parametrization-thoughts-, in: Proceedings of the 35th RD50 Workshop on Radiation Hard Semiconductor Devices for Very High Luminosity Colliders, Zurich, Switzerland, 2019 Nov[Online]. Available:.
[15] M. Moll, Acceptor removal - displacement damage effects involving the shallow acceptor doping of p-type silicon devices, in: Proceedings of Science 373, 027 - the 28th International Workshop on Vertex Detectors (Vertex2019) - Radiation effects, Sissa Medialab, 2020 [Online] Available:.
[16] F. Moscatelli, D. Passeri, A. Morozzi, G.F.D. Betta, R. Mendicino, G.M. Bilei, Combined bulk and surface radiation damage effects at very high fluences in silicon detectors: measurements and TCAD simulations, IEEE Trans. Nucl. Sci. 63 (5) (2016) 2716–2723.
[17] R. Dalal, A. Bhardwaj, K. Ranjan, K. Lalwani, G. Jain, Simulation of irradiated Si detectors, in: Proceedings of Science 227, 030 - the 23rd International Workshop on Vertex Detectors (Vertex2014) - R&D and Detector Simulations, Sissa Medialab, 2015 [Online] Available:.
[18] M. Raine, A. Jay, N. Richard, V. Goiffon, S. Girard, M. Gaillardin, P. Paillet, Simulation of single particle displacement damage in silicon - part I: global approach and primary interaction simulation, IEEE Trans. Nucl. Sci. 64 (1) (2017) 133–140.
[19] A. Jay, M. Raine, N. Richard, N. Mousseau, V. Goiffon, A. Hémeryck, P. Magnan, Simulation of single particle displacement damage in silicon - part II: generation and long-time relaxation of damage structure, IEEE Trans. Nucl. Sci. 64 (1) (2017) 141–148.
[20] A. Jay, A. Hémeryck, N. Richard, L. Martin-Samos, M. Raine, A.L. Roch, N. Mousseau, V. Goiffon, P. Paillet, M. Gaillardin, P. Magnan, Simulation of single-particle displacement damage in silicon - part III: first principle characterization of defect properties, IEEE Trans. Nucl. Sci. 65 (2) (2018) 724–731.
[21] P. López, M. Aboy, I. Muñoz, I. Santos, L.A. Marqués, P. Fernández-Martínez, M. Ullán, L. Pelaz, Atomistic simulations of acceptor removal in p-type Si irradiated with neutrons, Nucl. Instrum. Methods Phys. Res. B 512 (2022) 42–48.
[22] L. Snoj, G. Žerovnik, A. Trkov, Computational analysis of irradiation facilities at the JSI TRIGA reactor, Appl. Radiat. Isot. 70 (2012) 483.
[23] A. Ruzin, Recent results from the RD-48 (ROSE) collaboration, Nucl. Instrum. Methods Phys. Res. A 447 (2000) 116–125.
[24] M.R. Gilbert, J. Marian, J.-Ch. Sublet, Energy spectra of primary knock-on atoms under neutron irradiation, J. Nucl. Mater. 467 (2015) 121–134.
[25] M.T. Robinson, I.M. Torrens, Computer simulation of atomic displacement cascades in solids in the binary-collision approximation, Phys. Rev. B 9 (1974) 5008–5024.
[26] M. Jaraiz, L. Pelaz, J.E. Rubio, J. Barbolla, G.H. Gilmer, D.J. Eaglesham, H.J. Gossmann, J.M. Poate, Atomistic modeling of point and extended defects in crystalline materials, Mater. Res. Soc. Symp. Proc. 532 (1998) 43–53.
[27] M. Aboy, I. Santos, L. Pelaz, L.A. Marqués, P. López, Modeling of defects, dopant diffusion and clustering in silicon, J. Comput. Electron. 13 (2014) 40–58.
[28] L. Pelaz, V.C. Venezia, H.-J. Gossmann, G.H. Gilmer, A.T. Fiory, C.S. Rafferty, M. Jaraiz, J. Barbolla, Activation and deactivation of implanted B in Si, Appl. Phys. Lett. 75 (1999) 662–664.
[29] R. Pinacho, P. Castrillo, M. Jaraiz, I. Martin-Bragado, J. Barbolla, H.-J. Gossmann, G.H. Gilmer, J.L. Benton, Carbon in silicon: modeling of diffusion and clustering mechanisms, J. Appl. Phys. 92 (2002) 1582.
[30] G. Kissinger, J. Dabrowski, T. Sinno, Y. Yang, D. Kot, A. Sattler, *Ab initio* calculations and rate equation simulations for vacancy and vacancy-oxygen clustering in silicon, J. Cryst. Growth 468 (2017) 424–432.
[31] M. Kuhnke, E. Fretwurst, G. Lindström, Defect generation in crystalline silicon irradiated with high energy particles, Nucl. Instrum. Methods Phys. Res. B 186 (2002) 144–151.
[32] M. Moll, H. Feick, E. Fretwurst, G. Lindström, C. Schütze, Comparison of defects produced by fast neutrons and ^{60}Co-gammas in high-resistivity silicon detectors using deep-level transient spectroscopy, Nucl. Instrum. Methods Phys. Res. A 388 (1997) 335–339.
[33] B.C. MacEvoy, G. Hall, K. Gill, Defect evolution in irradiated silicon detector material, Nucl. Instrum. Methods Phys. Res. A 374 (1996) 12–26.
[34] P.D. de Almeida, Measurement of the acceptor removal rate in silicon pad diodes, in: Proceedings of the 30th RD50 Workshop Radiation Semiconductor Devices Frovery High Luminosity Colliders, Krakow, Poland, 2017 Jun[Online]. Available:.
[35] P. Fernández-Martínez, D. Flores, S. Hidalgo, X. Jordà, X. Perpiñà, D. Quirion, L. Ré, M. Ullán, M. Vellvehí, A new vertical JFET power device for harsh radiation environments, Energies 10 (2017) 256.
[36] M. Moll, E. Fretwurst, G. Lindström, Investigation on the improved radiation hardness of silicon detectors with high oxygen concentration, Nucl. Instrum. Methods Phys. Res. A 439 (2000) 282–292.

[37] M. Moll, Displacement damage in Si detectors for high energy physics, IEEE Trans. Nucl. Sci. 65 (2018) 1561–1582.
[38] B. Hiti, V. Cindro, A. Gorišek, T. Hemperek, T. Kishishita, G. Kramberger, H. Krüger, I. Mandić, M. Mikuž, N. Wermes, M. Zavrtanik, Charge collection properties in an irradiated pixel sensor built in a thick-film HV-SOI process, J. Instrum. 12 (2017) P10020.
[39] G. Kramberger, Reasons for high charge collection efficiency of silicon detectors at HL-LHC, Nucl. Instrum. Methods Phys. Res. A 924 (2019) 192–197.
[40] J.L. Lindström, L.I. Murin, V.P. Markevich, T. Hallberg, B.G. Svensson, Vibrational absorption from vacancy-oxygen-related complexes (VO, V_2O, VO_2) in irradiated silicon, Phys. B Condens. Matter 273–274 (1999) 291–295.
[41] P.A. Stolk, D.J. Eaglesham, H.-J. Gossmann, J.M. Poate, Carbon incorporation in silicon for suppressing interstitial-enhanced boron diffusion, Appl. Phys. Lett. 66 (1995) 1370.
[42] L.C. Kimerling, M.T. Asom, J.L. Benton, P.J. Drevinsky, C.E. Caefer, Interstitial defect reactions in silicon, Mater. Sci. Forum 38–41 (1989) 141–150.
[43] P.M. Mooney, L.J. Cheng, M. Süli, J.D. Gerson, J.W. Corbett, Defect energy levels in boron-doped silicon irradiated with 1-MeV electrons, Phys. Rev. B 15 (1977) 3836.
[44] K. Lauer, C. Möller, D. Schulze, C. Ahrens, J. Vanhellemont, Discussion of A_{Si}-Si_i-defect model in frame of experimental results on P line in indium doped silicon, Solid State Phenom. 242 (2015) 90–95.
[45] C. Besleaga, A. Kuncser, A. Nitescu, G. Kramberger, M. Moll, I. Pintilie, Bistability of the B_iO_i complex and its implications on evaluating the "acceptor removal" process in *p*-type silicon, Nucl. Instrum. Methods Phys. Res. A 1017 (2021) 165809.
[46] G. Hobler, L. Pelaz, C.S. Rafferty, Continuum treatment of spatial correlation in damage annealing, Nucl. Instr. Methods Phys. Res. B 153 (1999) 172–176.
[47] V. Cindro, G. Kramberger, M. Lozano, I. Mandic, M. Mikuž, G. Pellegrini, J. Pulko, M. Ullan, M. Zavrtanik, Trapping of electrons and holes in *p*-type silicon irradiated with neutrons, in: Proceedings of the 15th International Workshop on Room-Temperature Semiconductor X- and Gamma-Ray Detectors, IEEE Nuclear Science Symposium Conference Record, 2006, pp. 139–142. N09-2.
[48] K. Gill, G. Hall, B. MacEvoy, Bulk damage effects in irradiated silicon detectors due to clustered divacancies, J. Appl. Phys. 82 (1997) 126.
[49] E. Holmström, K. Nordlund, M. Hakala, Amorphous defect clusters of pure Si and type inversion in Si detectors, Phys. Rev. B 82 (2010) 104111.
[50] P. Santos, J. Coutinho, M.J. Rayson, P.R. Briddon, Electrical activity of multivacancy defects in silicon, Phys. Status Solidi C 9 (2012) 2000–2004.
[51] I. Santos, M. Aboy, P. López, L.A. Marqués, L. Pelaz, Insights on the atomistic origin of X and W photoluminescence lines in c-Si from *ab initio* simulations, J. Phys. D Appl. Phys. 49 (2016) 075109.
[52] A. Carvalho, R. Jones, J. Coutinho, P.R. Briddon, Density-functional study of small interstitial clusters in Si: comparison with experiments, Phys. Rev. B 72 (2005) 155208.
[53] S. Saramad, A new explanation for some open questions of hadron irradiated silicon detectors, Nucl. Instrum. Methods Phys. Res. A 510 (2003) 101–106.
[54] V.P. Markevich, A.R. Peaker, S.B. Lastovskii, L.I. Murin, J. Coutinho, V.J.B. Torres, P.R. Briddon, L. Dobaczewski, E.V. Monakhov, B.G. Svensson, Trivacancy and trivacancy-oxygen complexes in silicon: experiments and *ab initio* modeling, Phys. Rev. B 80 (2009) 235207.
[55] M. Moll, E. Fretwurst, M. Kuhnke, G. Lindström, Relation between microscopic defects and macroscopic changes in silicon detector properties after hadron irradiation, Nucl. Instrum. Methods Phys. Res. B 186 (2002) 100–110.